Machine Copy for Proofreading, Vol. x, y–z, 2013

A PHYSICAL OPTICS APPROACH TO THE ANALYSIS OF LARGE FREQUENCY SELECTIVE RADOMES

Ugo d'Elia[1], Giuseppe Pelosi[2], Christian Pichot[3], Stefano Selleri[2, *], and Massimo Zoppi[2, 3]

[1]MBDA Italia S.p.A., Missile Systems, Via Tiburtina Km 12.400, Rome, Italy

[2]Department of Information Engineering, University of Florence, Via di Santa Marta 3, I-50139 Florence, Italy

[3]Laboratory of Electronics, Antennas and Telecommunications (LEAT), University of Nice-Sophia Antipolis, CNRS UMR 6071, Valbonne 06560, France

Abstract—State-of-the-art radomes exploit frequency selective media so as to be transparent for the frequencies of the antenna protected by them and opaque to other frequencies. This feature helps in reducing the radar cross section of the antenna and in protecting it from interference. The study of a frequency selective radome is a daunting task, since the radome is usually large in terms of wavelengths, hence full wave analyses are prohibitive. In this paper an approximate technique, based on the physical optics concept, is proposed to attain an estimation of the behavior of a radome shielded antenna in a short time with a commonly available computer. Results are validated against a full wave technique over a relatively small radome.

1. INTRODUCTION

The study of the effects of radomes over the electromagnetic characteristics of the shielded antenna has attracted the interest of researchers and industries since long. Depointing, gain decrease and side lobe level variation must be accurately predicted to maintain system performances at the desired level.

For large radomes ray-tracing techniques have been the first to be applied, as, for example, in [1–4]. Method of moments (MoM) has also

Received 28 January 2013.

* Corresponding author: Stefano Selleri (stefano.selleri@unifi.it).

been used [5–7], possibly accelerated via a fast multipole method [8], as well as finite element method (FEM) [9]. More recently hybrid techniques mixing PO and MoM for low curvature parts and full-wave MoM method for the high curvature parts [10–12], or mixing PO, boundary integrals, mode matching and FEM [13] were investigated. For particular geometries, analytic methods are also possible [14].

The above mentioned methods were developed and applied to homogeneous radomes, but modern radomes for radars are often required to present a frequency dependent behavior, for screening the radar transmitting/receiving antenna from hostile emissions, yet allowing the frequencies in the band of the protected radar to pass through [15, 16]. Such radomes can be built embedding a frequency selective surface (FSS), usually realized by a periodic arrangement of some sort of base unit cell, able to operate a frequency filtering on the incident radiation [17]. The presence of the FSS usually disrupt any body of revolution symmetry the radome may exhibit and on which some of the aforementioned techniques are based to attain a higher efficiency.

FSS have found wide use in various applications, not only radar antennas; but also to absorb an incident radiation and hence reduce the radar cross section of a target [18, 19]; to provide a reflective surface for beam focusing in reflector antenna system [20–22] or to enhance array antenna performances [23].

While the analysis of planar infinite FSS is well established and design techniques do exist, usually based on a Floquet mode expansion over a single periodic cell [17, 24–27], a frequency selective radome exploits a finite, curved, FSS. The study of curved and finite FSS, especially for radomes, is matter of active research since the influence of the radome over the antenna characteristics is stronger than in the homogeneous radome case. Analysis is usually done, in open literature, by resorting to geometrical optics (GO) approximation. This requires the knowledge of both the transmission and reflection coefficients related to the equivalent planar and infinite FSS, computed over a wide range of possible incidence angles and polarizations. Then the curved or finite FSS is treated in a ray-tracing framework, and to each ray the pertinent reflection and transmission coefficient is applied — possibly taking into account multiple internal reflections [28–31]. Alternate approaches relies on equivalent impedance boundary conditions which are, anyway, computed on the equivalent, planar, infinite, FSS [32]. Yet the problem of the curved FSS of a radome is critical since the surface periodicity is disrupted as the periodic cell cannot be deformed without significantly altering its frequency behavior and hence Floquet theory cannot be applied at all; applications to curved FSS, when available,

are anyway limited or quite complex to implement [33].

The analysis method suggested in this paper aims to improve the approximation of the GO-based methods, over curved FSS structures, using a technique based on the physical optics (PO) concept akin to the one in [10, 11] differing from cited papers in the way in which equivalent currents are computed which allow, in the present case, to treat frequency selective surfaces. Although PO is usually employed for conducting bodies, it has been extended also to penetrable structures [10, 11, 34]. In this paper a further extension is presented, attained by performing a high frequency approximation of the currents induced over the FSS and letting them radiate. Such approximation is performed by exploiting the already mentioned and accurate FE techniques for planar infinite FSS [26, 27]. This under the hypothesis that currents computed on the planar, infinite, FSS are an acceptable approximation of the equivalent currents which would be present on the non-uniform and non-planar FSS of the radome.

A similar PO-based approach for FSS radomes was suggested for the first time in [35], where the equivalent current were computed on the basis of the simple GO approach over a uniform surface exhibiting the reflection coefficient of the FSS. In this paper, instead, equivalent currents are considered non-uniform and numerically computed via a full wave FE simulation.

A more accurate analysis could be performed by hybridizing PO with MoM as it is done in [11] for homogeneous radomes, but this would be necessary only if the curvature radius of the radome becomes small, as for the pointed radome analyzed in [11], and at a very high computational price.

The paper is organized as follows: subsequent Section 2 briefly summarize the PO approximation, with particular attention to the curved FSS problem, comprehensive of a brief description of the FE-based method exploited to compute the equivalent currents; Section 3 presents the complete PO implementation over a typical paraboloidal homogeneous radome; Section 4 presents numerical results and validations and finally Section 5 draws some conclusions.

2. PO APPROXIMATION OF A FSS

Let's consider a generic FSS, comprising one or possibly several layers of periodically arranged perfectly conducting patches or of slots in a perfectly conducting sheet, possibly embedded in a stratified dielectric medium (Fig. 1).

Such a structure, illuminated by an impinging plane wave $\mathbf{E}_i$ forming an angle θ_i with the normal to the surface can be efficiently

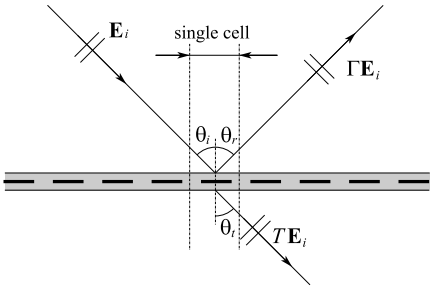

Figure 1. Generic planar infinite FSS, with single periodic cell highlighted.

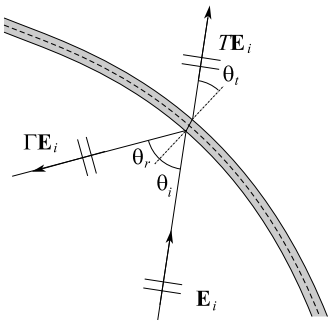

Figure 2. Simple GO approach to curved FSS scattering.

analyzed on the basis of a single periodic cell via FE by enforcing periodicity conditions at cell sides and an appropriate expansion in Floquet harmonics above and beneath the cell [27]. Transmitted and reflected field is then given as a summation of Floquet modes but, if the periodic cell is half a wavelength or smaller, then only the fundamental Floquet modes, directed as $\theta_t = \theta_i$ and $\theta_r = \theta_i$ are propagating and hence transmitted and reflected fields far from the FSS can be treated as single plane waves of amplitudes $T\mathbf{E}_i$ and $\Gamma\mathbf{E}_i$, respectively.

In this framework a first simple approximation of a curved FSS consists in performing a ray trace and employing the pertinent values for coefficient T and Γ for the local incidence angle (Fig. 2).

In a PO approach, on the other hand, the field on the surface can be exploited to compute equivalent currents whose radiated field approximate the actual scattered field. In a full wave FE approach total fields are computed very accurately on a periodic cell, considering all the necessary Floquet harmonics, and can be used easily to recover the equivalent surface currents of the PO approach, on both side of the FSS, inner ($\mathbf{J}_s^{(i)}$ and $\mathbf{M}_s^{(i)}$) and outer ($\mathbf{J}_s^{(o)}$ and $\mathbf{M}_s^{(o)}$) (Fig. 3). Such equivalent currents can then be used to approximate the corresponding equivalent currents on a curved FSS on a cell-by-cell basis, computing the angle of incidence of the ray impinging on the center of the cell and solving the planar infinite problem for that ray (Fig. 4).

The analysis of a planar periodic structures via a hybrid FE-Floquet Modes procedure is well established and need not to be detailed here [26, 27].

The full-wave analysis results can easily lead to the fields over a desired surface parallel to the FSS. In the case of dielectric coated FSS this surface should be chosen coincident with the outer air-dielectric

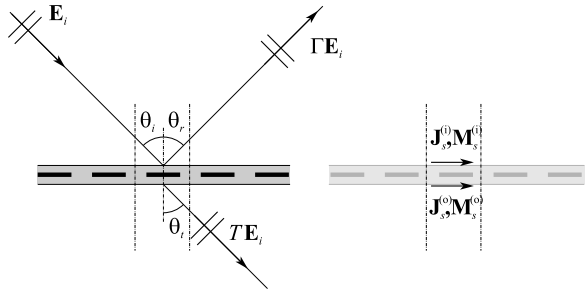

Figure 3. Evaluation of the equivalent electric ($\mathbf{J}_s^{(i,o)}$) and magnetic ($\mathbf{M}_s^{(i,o)}$) currents in a FE approach.

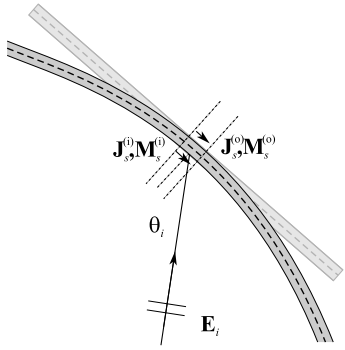

Figure 4. Curved FSS (black) and corresponding infinite planar FSS for the single cell under analysis.

interface, while in case of a only-metallic FSS the choice of the metal-air interface might lead to substantial reduction of computational burden due to the fact that only the fields at the slots in the FSS, and the pertinent equivalent currents, need to be considered.

From the fields the equivalent electric and magnetic currents at the chosen equivalent surface can be obtained via the well known relations

$$\mathbf{J}_s^{(i,o)} = \mathbf{n}^{(i,o)} \times \mathbf{H}^{(i,o)} \tag{1}$$

$$\mathbf{M}_s^{(i,o)} = \mathbf{E}^{(i,o)} \times \mathbf{n}^{(i,o)} \tag{2}$$

PO theory is very well established, and has been applied also to penetrable bodies [10, 11]. Here we propose a PO method applied over a curved and truncated FSS: this leads to a further approximation with respect to the classic PO method but, at the same time, permits an extremely fast numerical analysis for the curved and truncated FSS. The introduced approximation lies in the loss of periodicity on

the curved FSS with respect to the infinite planar one on which PO currents are estimated. Notwithstanding the disrupted periodicity, the general behavior of the FSS is not so much affected when applied on a curved surface, as the results in the following will show.

3. PO ANALYSIS OF A RADOME

The analysis of a curved radome requires, as a first step, the mapping of the unit FSS cells over the curved radome. This cannot be a conformal mapping since cell dimension cannot vary not to spoil frequency behavior, hence an arrangement of the unmodified cells is required. In the following, without loss of generality, a paraboidal radome of diameter D and height h will be considered (Fig. 5).

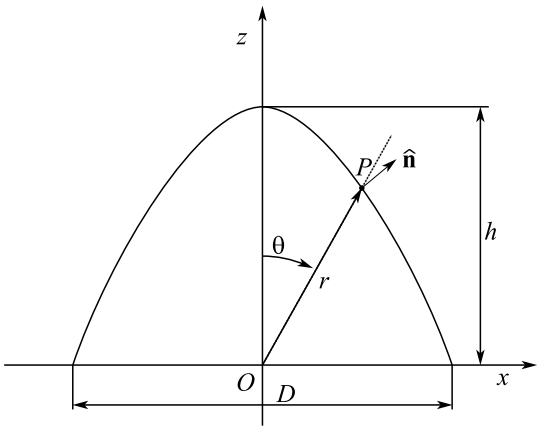

Figure 5. Paraboloidal radome. A generic point $P(r, \theta)$ and the pertinent normal is also shown. The paraboloidal is of revolution with respect to the z axis and hence ϕ independent.

In the present approach a single cell will be placed on the tip of the paraboloidal radome, and concentric rings of cells will be arranged around it trying to keep the distance between cells as uniform as possible and its distributions as symmetric as possible. Every cell position is determined by its central point P in a spherical reference (r, θ, ϕ) (Fig. 6). Since the map process doesn't depend on the geometry of the unitary cell, if the geometry of the radome does not vary several different FSS can be analyzed without having to recompute mappings. In particular, a homogeneous radome can be analyzed if the unit cell contains only a homogeneous dielectric.

The source within the radome can be either a single source of a given pattern or, more generally, an array of radiating elements. This

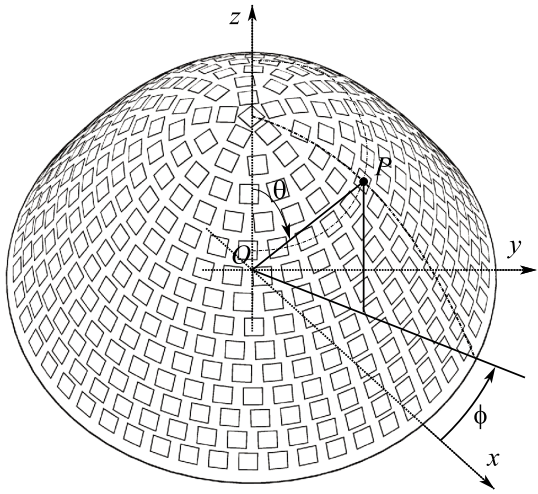

Figure 6. Disposition of cells over a paraboloidal radome. Cells are arranged in concentric rings around the radome tip. A generic cell, centered in $P(r, \theta, \phi)$ is highlighted.

second case will be explicitly treated in the following. The generic source S, be it single or an element of an array, is placed in (r', θ', ϕ') and oriented according to its own local reference $(\hat{\mathbf{x}}_S, \hat{\mathbf{y}}_S, \hat{\mathbf{z}})_S$ (Fig. 7).

Once the cell distribution is fixed and the inner source placed a ray-tracing procedure is performed devising all possible source-cell pairs. For each the mutual distance R and relative orientation is computed. The direction $\hat{\mathbf{k}}$ of the segment joining S to P and the normal to the radome $\hat{\mathbf{n}}$ define the plane of incidence of the wave (gray in Fig. 7). On this basis a pair of incidence angles θ_i and ϕ_i can be defined (Fig. 8), as well as an appropriate parallel $\hat{\mathbf{v}}_{//}$ and perpendicular $\hat{\mathbf{v}}_{\perp}$ direction of polarization onto which decompose the generic incident wave generated in S. All these geometrical data is quite straightforward to compute and numerical details are omitted for the sake of brevity. If the source in the radome is an array then the computations are repeated for every element in the array. All the data is finally stored in a look-up table.

The data set can be conveniently decimated by allowing only discrete steps in the incidence angles on the radome cells. This will significantly reduce the amount of FE computations without a sensible loss of accuracy, as numerical results will show.

Once a look-up table of incidence angles is built, two full wave simulations are performed for each element in the set, one for a unitary TE (perpendicular polarization) impinging plane wave and one for a

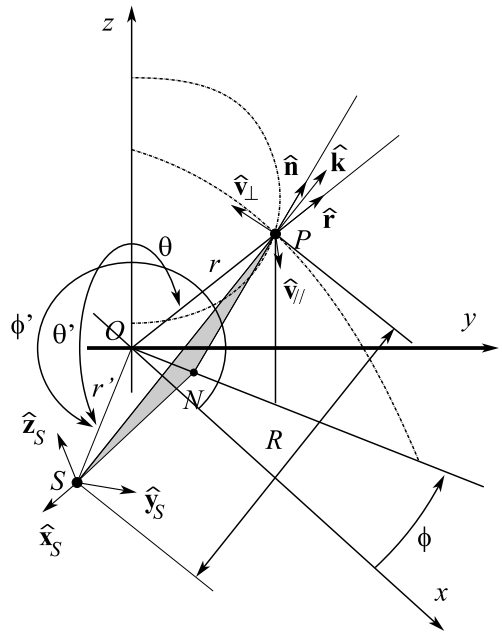

Figure 7. Relative positioning of a generic cell source $S(r', \theta', \phi')$ and its local reference ($\hat{\mathbf{x}}_S$, $\hat{\mathbf{y}}_S$, $\hat{\mathbf{z}}_S$ and a generic cell located in $P(r, \theta, \phi)$. The gray triangle shows the incident plane defining the directions of parallel ($\hat{\mathbf{v}}_{//}$) and perpendicular ($\hat{\mathbf{v}}_\perp$) polarization.

unitary TM (parallel polarization) impinging plane wave. From the so-obtained fields equivalent currents over the chosen surface are extracted and stored. These currents are sampled over a convenient finite number of points.

The subsequent step consists in finding, in the already computed ray-tracing GO approximation, the polarization, amplitude and phase of any ray impinging from any single source over any radome cell. These quantities are used as weights for the electric and magnetic currents for the pertinent configuration of polarization and incident angles.

All the weighted currents from all sources relative to a single unit cell are then summed up and placed in the correct 3D position. This procedure leads to a complete surface distribution of equivalent electric and magnetic currents on the outer surface of the radome.

Once such a distribution is obtained a radiation integral over this discrete current samples leads to the radiated field through the radome.

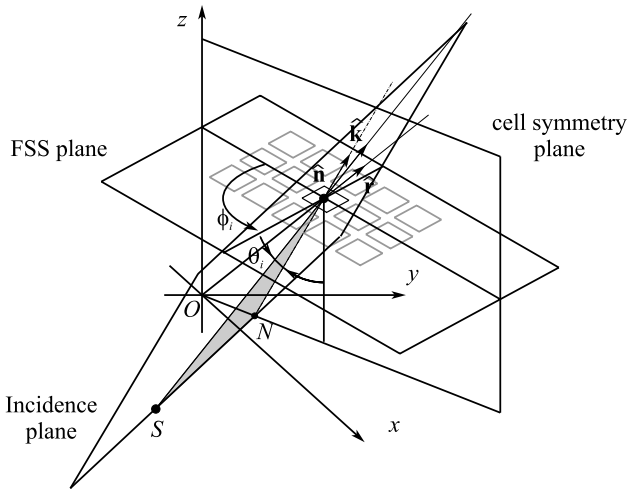

Figure 8. Angles of incidence over the single cell in P: angle θ_i is the inclination (angle between the normal to the surface $\hat{\mathbf{n}}$ and the direction of the impinging ray $\hat{\mathbf{k}}$); angle ϕ_i is the rotation angle (angle between the incident plane defined by $\hat{\mathbf{n}}$ and $\hat{\mathbf{k}}$ and the symmetry plane of the single cell, containing the vertical axis z and passing through P).

4. NUMERICAL RESULTS

In this section the results for a paraboloidal radome both in the homogeneous and FSS cases are presented. Geometrical characteristics are sketched in Table 1 and Fig. 5.

Table 1. Test radome geometry.

Quantity	Value
Diameter D	150 mm
Height h	90 mm
Cell rings	15
Number of Cells	426
Array elements	37

The geometry has been chosen because it is the biggest the authors managed to solve also via a full wave commercial solver (Microwave Studio CST), yet smaller radomes would have been a poorer comparison because unrealistic and because the proposed PO

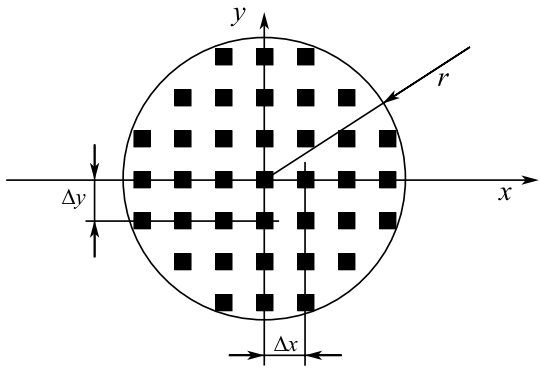

Figure 9. Radiating array.

technique is accurate for large radomes. It must be noted that the structure contains very fine slots and that CST reported few discretization errors which couldn't be solved with a finer mesh due to memory limitations.

The antenna inside the radome is an array of $N = 37$ elements arranged in a regular square grid with $\Delta x = \Delta y = \lambda_0/2$ (Fig. 9). The working frequency being 11.5 GHz, it is $\lambda_0 = 26.1$ mm. The elements, considered isotropic, are arranged in an octagonal shape so as to be within a circle of radius $r = 45$ mm, with equal amplitudes and linear phases chosen so that the array θ_0 pointing angle scans from 0 to 15° (Fig. 10).

First, to validate the technique against GO and CST, a homogeneous radome is analyzed. Numerical results are computed for the above defined array pointing at broad side ($\theta_0 = 0$) or with an electronic $\theta_0 = 15°$ tilt. Results are plotted in Figs. 11 and 12, respectively. The GO solution, which is quite inaccurate, basically mimics the pattern of the array without any radome, whereas the PO solution, even if with appreciable difference with respect to the full wave CST solution, is much closer to this latter, both for what concerns the main lobe shape and the side lobe level.

Then, the radome of Table 1 and Fig. 5 is analyzed, with the same array source. Results are again given for GO, for the proposed PO technique, and for CST, for broadside pointing and for a 15° tilt (Figs. 13 and 14).

Again, good agreement between the proposed method and the full wave solution can be seen, especially for the prediction of side lobes. To gain a further insight on the effects of the radome, Figs. 15 and 16 shows a zoom on the main beam. In broadside direction (Fig. 15)

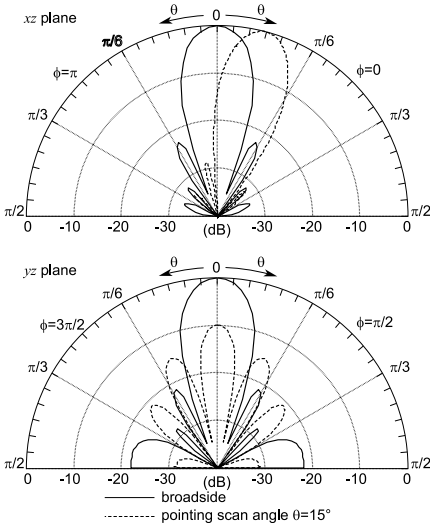

Figure 10. Array radiation patterns, without radome, for a pointing scan angle of 0 (broadside) and 15°.

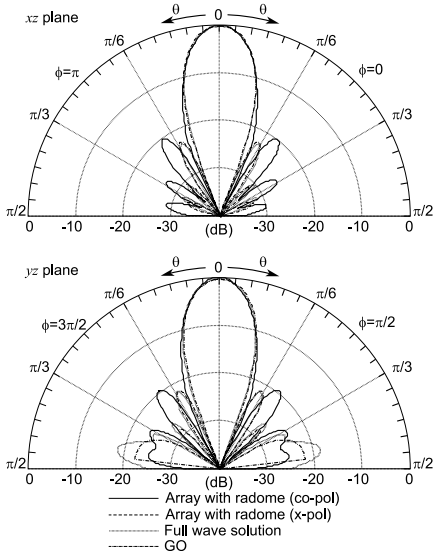

Figure 11. Radiation patterns for the broadside array without the homogeneous radome and with the homogeneous radome, computed with the proposed PO technique and via a full-wave solver.

a slight reduction of the beamwidth can be observed, while for the $\theta = 15°$ pointing scan it can be noted (Fig. 2) how two solutions (PO and Full-wave) differs by only a couple of degrees in the direction of maximum radiation. This value, in terms of half power beamwidth, is about 10%. It must anyway be stressed that the proposed approach is approximate and it has been developed to produce fast results with a reasonable accuracy.

To further investigate the pattern produced by the different approaches, Table 2 shows the half power beamwidth of the original 37 elements array and how it is affected by the radome presence either computed via GO, the proposed PO technique or a full wave CST run. It is apparent how the values, at broadside or at a 15° tilt are comparable.

Table 3 shows the gain of the array without radome and the gain of the array protected by the radome computed with GO, PO and CST both pointing at broad side ($\theta = 0$) or with a $\theta = 15°$ tilt. Again values are quite close one to the other.

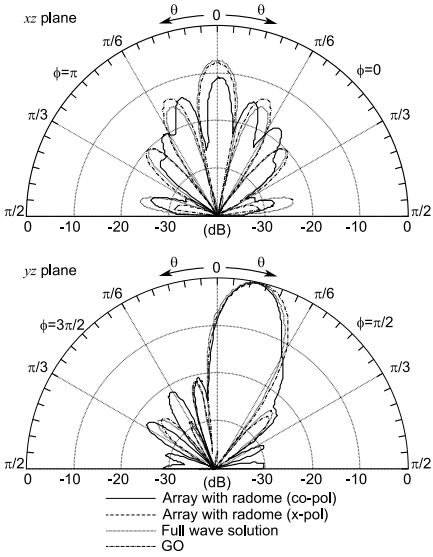

Figure 12. Radiation patterns for the phased array pointing at ($\phi_0 = 90°$, $\theta_0 = 15°$) without the homogeneous radome and with the homogeneous radome, computed with the proposed PO technique and via a full-wave solver.

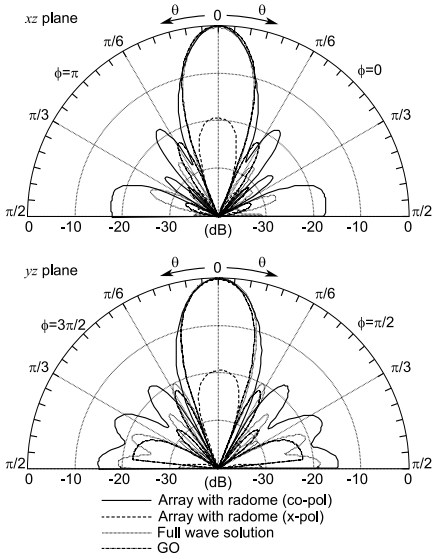

Figure 13. Radiation patterns for the broadside array without the radome and with the radome, computed with the proposed PO technique and via a full-wave solver.

Table 2. Half power beam width (HPBW).

Pointing	Plane	Array	GO	PO	CST
Broad Side	$V\ (\phi = 0)$	17.24°	17.47°	14.57°	17.00°
	$H\ (\phi = \pi/2)$	17.70°	17.47°	17.90°	16.35°
$\theta_0 = 15°$	$V\ (\phi = 0)$	17.58°	17.57°	14.50°	17.50°
$\phi_0 = 90°$	$H\ (\phi = \pi/2)$	17.95°	18.21°	19.89°	16.80°

Table 3. Gain.

	Array	GO	PO	CST
Pointing $\theta = 0°$	21.44	22.37	20.14	21.12
Pointing $\theta = 15°$	21.56	21.50	20.31	20.86

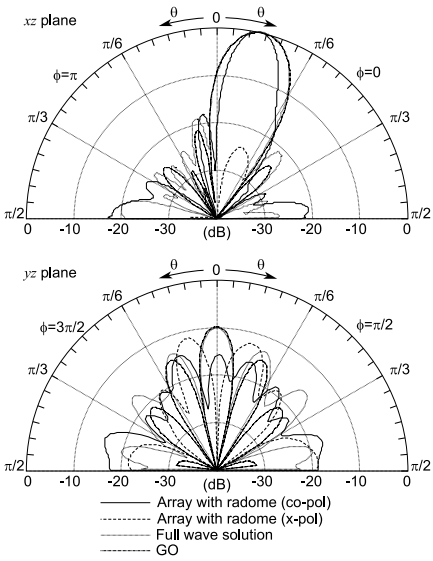

Figure 14. Radiation patterns for the phased array pointing at ($\phi_0 = 90°$, $\theta_0 = 15°$) without the radome and with the radome, computed with the proposed PO technique and via a full-wave solver.

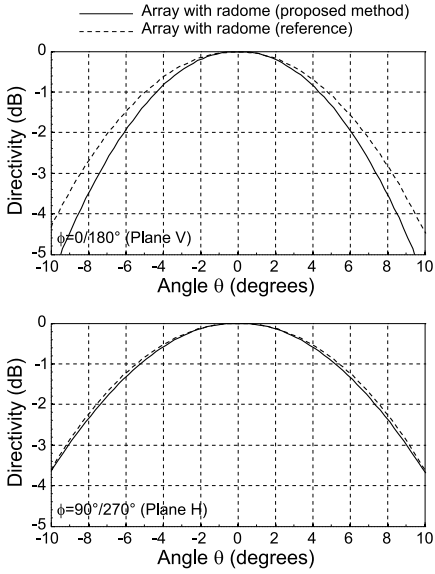

Figure 15. Zoom over the main beam for the phased array with broadside pointing, with the radome, computed with the proposed PO technique and via a full-wave solver.

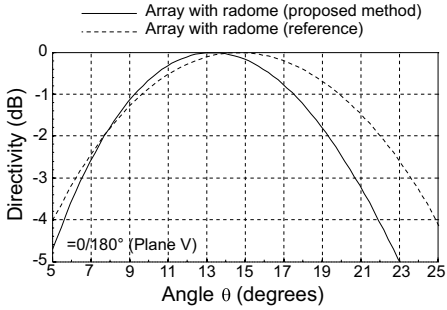

Figure 16. Zoom over the main beam for the phased array pointing at ($\phi_0 = 90°$, $\theta_0 = 15°$) with the radome, computed with the proposed PO technique and via a full-wave solver.

In both Tables 2 and 3 PO and GO gives similar results, GO being faster, but this is due to the fact that both tables reports quantities bound to the main beam, which GO models fairly accurately. More interesting is Table 4, which clearly shows how PO better models fields

Table 4. Side lobe level (SLL).

	Array	GO	PO	CST
Pointing $\theta = 0°$	-22.52	-21.47	$-16,50$	$-18,62$
Pointing $\theta = 15°$	-21.74	-21.48	-18.25	-18.85

Table 5. CPU time and memory occupation comparison.

		PO	CST
CPU time (s)	Pre-processing	359	394969
	Eq. currents database	9524	
	Mapping and Radiation	4205	
	Total	14088	
		PO w.r. to CST 3.57%	
Memory (kB)	Pre-processing	524627	7075744
	Eq. currents database	624995	
	Mapping and Radiation	1327216	
	Total	2476838	
		PO w.r. to CST 35.00%	
Disk (MB)		312	8840
		PO w.r. to CST 35.29%	

far from the main beam, that is the side lobe level (SLL). Indeed Figs. 13 and 14 do also show how PO approximate better the shape of the radiation diagram outside the main beam, which can be cause of serious issue in radar installation.

Finally, Table 5 shows the different requirements, in terms of CPU time, memory and disk, of the proposed PO approach and the full-wave solution. It is evident how the test radome can be analyzed with the proposed PO technique over a standard PC in relatively short times, while the full-wave solution requires a powerful workstation for many hours. In particular, for this particular problem, the proposed technique is about 28 times faster than CST. Of course much larger radomes can be analyzed via PO.

5. CONCLUSIONS

An approximate PO-based technique has been presented for the analysis of FSS radomes. The analysis relies on equivalent PO currents

numerically evaluated via a full wave FEM analysis on a single periodic cell.

The numerical results match well with those obtained via a full wave analysis of the whole radome, for a radome small enough to allow a full wave analysis, yet the PO-based algorithm required a negligible fraction of time and memory with respect to the full wave method.

REFERENCES

1. Paris, D., "Computer-aided radome analysis," *IEEE Trans. on Antennas and Propag.*, Vol. 18, 7–15, 1970.
2. Einziger, P. and L. Felsen, "Ray analysis of two-dimensional radomes," *IEEE Trans. on Antennas and Propag.*, Vol. 31, 870–884, 1985.
3. Gao, X. and L. Felsen, "Complex ray analysis of beam transmission through two-dimensional radomes," *IEEE Trans. on Antennas and Propag.*, Vol. 33, 963–975, 1985.
4. Orta, R., R. Tascone, and R. Zich, "Performance degradation of dielectric radome covered antennas," *IEEE Trans. on Antennas and Propag.*, Vol. 36, 1707–1713, 1988.
5. Harington, R. and J. Mautz, "An impedance sheet approximation for thin dielectric shells," *IEEE Trans. on Antennas and Propag.*, Vol. 23, 531–534, 1975.
6. Arvas, E. and S. Ponnapali, "Scattering cross section of a radome of arbitrary shape," *IEEE Trans. on Antennas and Propag.*, Vol. 37, 655–658, 1989.
7. Arvas, E., A. Rahhalarabi, U. Pekel, and E. Gundogan, "Electromagnetic transmission through a small radome of arbitrary shape," *IEE Proc. H, Microw. Antenn. Propagat.*, Vol. 137, 401–405, 1990.
8. Meng, H. and W.-B. Dou, "Fast analysis of electrically large radome in millimeter wave band with fast multipole acceleration," *Progress In Electromagnetics Research*, Vol. 120, 371–385, 2011.
9. Gordon, R. and R. Mittra, "Finite element analysis of axisymmetric radomes," *IEEE Trans. on Antennas and Propag.*, Vol. 41, 975–981, 1993.
10. Zhongxiang, S. and J. Volakis, "A hybrid physical opticsmoment method for large nose radome antennas," *Proc. IEEE Antennas and Propagation Symposium*, 2554–2557, 1999.
11. Abdel Moneum, M., Z. Shen, J. Volakis, and O. Graham, "Hybrid

PO-MoM analysis of large axi-symmetric radomes," *IEEE Trans. on Antennas and Propag.*, Vol. 49, 1657–1666, 2001.

12. Hu, B., X.-W. Xu, M. He, and Y. Zheng, "More accurate hybrid PO-MoM analysis for an electrically large antenna-radome structure," *Progress In Electromagnetics Research*, Vol. 92, 255–265, 2009.
13. Meng, H. and W.-B. Dou, "A hybrid method for the analysis of radome-enclosed horn antenna," *Progress In Electromagnetics Research*, Vol. 90, 219–233, 2009.
14. Sukharevsky, O. and V. Vasilets, "Scattering of reflector antenna with conic dielectric radome," *Progress In Electromagnetics Research B*, Vol. 4, 159–169, 2008.
15. Pous, R. and D. Pozar, "A frequency-selective surface using aperture-coupled microstrip patches," *IEEE Trans. on Antennas and Propag.*, Vol. 39, 1763–1769, 1991.
16. Lin, B.-Q., F. Li, Q.-R. Zheng, and Y.-S. Zen, "Design and simulation of a miniature thick-screen frequency selective surface radome," *IEEE Antennas Wireless Propag. Lett.*, Vol. 8, 1065–1068, 2009.
17. Munk, B., *Frequency Selective Surfaces, Theory and Design*, John Wiley & Sons Inc., New York, NY, 2000.
18. Ford, K. and B. Chambers, "Improvement in the low frequency performance of geometric transition radar absorbers using square loop impedance layers," *IEEE Trans. on Antennas and Propag.*, Vol. 56, 133–141, 2008.
19. dElia, U., G. Pelosi, S. Selleri, and R. Taddei, "A carbon nanotube based frequency-selective absorber," *Int. J. Microw. Wireless Tech.*, Vol. 2, 479–485, 2010.
20. Rahmat-Samii, Y. and A. Tulintseff, "Diffraction analysis of frequency selective reflector antennas," *IEEE Trans. on Antennas and Propag.*, Vol. 41, 476–487, 1993.
21. Wu, T.-K. and S.-W. Lee, "Multiband frequency selective surface with multiring patch elements," *IEEE Trans. on Antennas and Propag.*, Vol. 42, 1484–1490, 1994.
22. Moore, E., "A 10–183 GHz common aperture antenna with a quasioptical frequency multiplexer," *Proc. Combined Optical-Microwave Earth and Atmosphere Sensing Symposium*, 220–222, 1995.
23. Erdemli, Y., K. Sertel, R. Gilbert, D. Wright, and J. Volakis, "Frequency-selective surfaces to enhance performance of broadband reconfigurable arrays," *IEEE Trans. on Antennas and*

Propag., Vol. 50, 1716–1724, 2002.

24. Zadeh, A. and A. Karlsson, "Capacitive circuit method for fast and efficient design of wideband radar absorbers," *IEEE Trans. on Antennas and Propag.*, Vol. 57, 2307–2314, 2009.
25. Munir, A., V. Fusco, and O. Malyunskin, "Tunable frequency selective surface characterization," *Proc. European Microwave Conference*, 813–816, 2008.
26. Cecchini, R., R. Coccioli, and G. Pelosi, "PERIODIC3: A software package for the analysis of artificially anisotropic surfaces," *IEEE Antennas Propag. Mag.*, Vol. 37, 84–86, 1995.
27. Pelosi, G., R. Coccioli, and S. Selleri, *Quick Finite Elements for Electromagnetic Waves*, 2nd Edition, Artech House, London, UK, 2009.
28. Parker, E., B. Philips, and R. Langley, "Ray tracing analysis of the transmission performance on curved FSS," *IEE Proc. Microwaves, Antennas Propagat.*, Vol. 142, 193–200, 1995.
29. Stanley, A. and E. Parker, "Ray tracing fields backscattered from curved dichroic structures," *IEE Proc. Microwaves, Antennas Propagat.*, Vol. 145, 406–410, 1998.
30. Pei, Y., A. Zeng, L. Zhou, R. Zhang, and K. Xu, "Electromagnetic optimal design for dual-band radome wall with alternating layers of staggered composite and kagome lattice structure," *Progress In Electromagnetics Research*, Vol. 122, 437–452, 2012.
31. Zhou, L., Y. Pei, R. Zhang, and D. Fang, "Optimal design for high-temperature broadband radome wall with symmetrical graded porous structure," *Progress In Electromagnetics Research*, Vol. 127, 1–14, 2012.
32. Stupfel, B. "Impedance boundary conditions for finite planar or curved frequency selective surfaces embedded in dielectric layers," *IEEE Trans. on Antennas and Propag.*, Vol. 53, 3654–3663, 2005.
33. Parker, E., B. Philips, and R. Langley, "Analysis of coupling between a curved FSS and an enclosed planar dipole array," *IEEE Microw. Guided Wave Lett.*, Vol. 5, 338–340, 1995.
34. Pelosi, G., G. Toso, and E. Martini, "PO field expression of a penetrable planar structure in terms of line integral," *IEEE Trans. on Antennas and Propag.*, Vol. 48, 1274–1276, 2000.
35. Bresciani, D. and S. Contu, "Scattering analysis of dichroic subreflectors," *Electromagnetics*, Vol. 5, 375–407, 1985.